

Measurement-Based Identification of Lumped Parameter Thermal Networks for sub-kW Outer Rotor PM Machines

Daniel Wöckinger*, Gerd Bramerdorfer*, Senior Member, IEEE, Stephan Drexler*, Silvio Vaschetto[§], Senior Member, IEEE, Andrea Cavagnino[§], Fellow, IEEE, Alberto Tenconi[§], Senior Member, IEEE, Wolfgang Amrhein*, and Frank Jeske†

Abstract—This work is on deriving precise lumped parameter thermal networks for modeling the transient thermal characteristics of electric machines under variable load conditions. The goal is to facilitate an accurate estimation of the temperatures of critical machines' components and to allow for running the derived model in real time to adapt the motor control based on the load history and maximum permissible temperatures. Consequently, the machine's capabilities can be exhausted at best considering a highly-utilized drive. The model shall be as simple as possible without sacrificing the exactness of the predicted temperatures. Accordingly, a specific lumped parameter thermal network topology was selected and its characteristics are explained in detail. The measurement data based optimization of its critical parameters through an evolutionary optimization strategy, and the therefore utilized experimental setup will be described in detail here. Measurement cycles were recorded for modeling and verification purposes including both static and dynamic test cycles with changing load torque and speed requirements. Applying the proposed hybrid approach for determining the model's parameters through involving physics-based equations as well as numerical optimization followed a significant improvement of the preciseness of the predicted motor temperatures compared to solely determining the networks's coefficients based on expert knowledge. Thereby, the validation included both the original measurement data as well as extra measurement runs. The proposed and applied strategy provides an excellent basis for future thermal modeling of electric machines.

Index Terms—electric machines, evolutionary algorithm, lumped parameter thermal network, optimization, outer rotor, permanent magnet synchronous machine

I. INTRODUCTION

Nowadays, electric machines are particularly optimized for any individual application. The variety of optimization scenarios is manifold, as different machine types, problem

Manuscript received Dec. 13, 2021; revised July 20, 2022; accepted Sep. 23, 2022.

This work has been supported by the COMET-K2 "Center for Symbiotic Mechatronics" of the Linz Center of Mechatronics (LCM) funded by the Austrian federal government and the federal state of Upper Austria.

D. Woeckinger, G. Bramerdorfer, S. Drexler, and W. Amrhein are with the Institute of Electrical Drives and Power Electronics, Johannes Kepler University Linz, Linz, Austria, e-mail: daniel.woeckinger@jku.at, gerd.bramerdorfer@jku.at, stephan.drexler@jku.at, wolfgang.amrhein@jku.at.

S. Vaschetto, A. Cavagnino, and Alberto Tenconi are with Dipartimento Energia, Politecnico di Torino, Italy, e-mail: silvio.vaschetto@polito.it, andrea.cavagnino@polito.it, alberto.tenconi@polito.it.

F. Jeske is with Ebm-papst St. Georgen GmbH & Co. KG, Germany, email: frank.jeske@de.ebm-papst.com

definitions, performance requirements, and methods for solving those problems are considered [2]–[5]. In the past, most of the electric machine optimization scenarios focused on the electromagnetic analysis, while other domains, e.g., the thermal or mechanical characteristics, were neglected or only a rough estimate was included. Now, evermore researchers focus on a multi-physics- or driving cycle based approach, as for instance presented in [6]–[8]. Besides, a system-level approach is frequently considered to capture the interaction of electric machine, power electronics, and control aspects [9].

It is essential to adapt the modeling approaches according to new manufacturing or cooling techniques and to allow for evermore detailed analyses. Accordingly, new techniques like oil spray based cooling of hairpin windings were recently treated [10]. New modeling approaches for specific components were developed, e.g., to characterize ball bearings utilized for electric machines [11]. Some authors further consider the thermal characteristics of electric machines in the presence of particular faults, like winding specific flaws [12], [13]. The winding generally is the focus of the work of many authors. For instance, there are also many activities regarding how to find a simple homogenized model for the volume where the winding is installed, including an equivalent representation of this domain with regard to the particular share of conductive material, insulation, and air [14]–[16].

To allow for fast evaluation of thermal characteristics, usually the modeling is focused on most important temperatures and heat flow paths. Research is done to minimize the thermal models' complexity while guaranteeing acceptable accuracy [17] or to automatize the (dynamic) model creation to some extent [18], [19]. In terms of thermal modeling, different approaches were introduced in the past. They can be categorized as follows:

- 1) Expert knowledge and physics-motivated based thermal modeling,
- 2) data based thermal modeling, e.g., by making use of machine learning or artificial intelligence techniques, and
- 3) a combination of (1) and (2).

Category (1) consists of modeling approaches where the model structure and respective coefficients, parameters, etc. are solely determined based on expert knowledge regarding the physical circumstances. Besides computing the quantities based



Fig. 1: Motor under test.

on machines' dimensions and materials' properties, auxiliary measurements used for calibration are sometimes taken into account. Nevertheless, the applied modeling techniques are always developed based on fundamentals from engineering science. Some examples can be found in [20]–[24].

Category (2) refers to approaches where the modeling is done without taking into account the physical circumstances in detail. In [25]–[29], corresponding recent activities are presented. The approaches allow for a higher flexibility in the model definition. For instance, by contrast to the first category, an indirect modeling of the temperatures, e.g., with regard to the machine's torque and speed, can be accomplished. Thus, no direct physical relation of model inputs and outputs is required. The derived models are often of black-box type, which can be unfavorable, because there is limited possibility for obtaining particular machine-specific information to gain insights. Thus, while for group (1), similar machine designs can be modeled with limited additional effort, for group (2), usually the modeling has to be started from scratch for any new design under consideration. Besides, it is very hard or even impossible to proof general stability of black-box models.

Category (3): this category finally embraces approaches where both, physical expertise, as well as new techniques from mathematics regarding modeling and optimization, as well as data-based information are taken into account. Some examples can be found in [30], [31].

Obviously, there are fluid boundaries among the categories. Throughout this work, the authors focus on category (3). A lumped parameter thermal network (LPTN) is selected based on expert knowledge for the outer rotor surface permanent magnet (SPM) machine under test. Afterwards, an optimization of critical parameters of the network is done using an evolutionary algorithm. The goal is to find the lowest possible temperature modeling errors. In order to minimize the runtime, the design space regarding the thermal network's parameters of the optimization problem is constrained based on engineering knowledge. The data for the model evaluation is obtained through measurements conducted by using an experimental setup.

This manuscript provides an extension of results initially published in [1]. The remaining content is organized as fol-

Outer rotor SPM	
Number of phases	3, Δ connection, phase coils II-connected
Number of pole pairs	2
Rotor outer diameter	68.4 mm
Axial length incl. flange	42.0 mm
Rated DC bus voltage	24 V
Rated DC bus current	5.1 A
Rated speed	7100 rpm
Rated torque	150 mNm
Terminal resistance (at 20 °C)	0.427 Ω

TABLE I: Characteristic motor data.

lows: in the next Section II, the motor under test is introduced. Section III presents the selected LPTN and discusses critical parameters and the residual settings for the applied modeling approach. Consequently, Section IV is about the experimental setup used for this work. Sample data obtained by measurements are presented for all considered machine components' temperatures. Expert-based calibration and optimization of parameters that are difficult to predict are presented in Section V. This is completed by a detailed comparison of modeling results versus additional measurements, which is extended to further measurement cycles not available at modeling stage in Section V-D. Finally, a summary and an outlook about future activities is illustrated in Section VI.

II. MOTOR UNDER TEST

In this paper, the thermal characteristics of a 3-phase, brushless SPM machine with outer rotor topology are studied. The motor with disassembled rotor is shown in Fig. 1. It has a rated power of 110 W at 150 mNm and 7100 rpm. Its most important data, as well as its electrical characteristics are summarized in Table I. One big challenge of creating a thermal model for this type of machine is the rotating rotor bell involving speed-dependent heat dissipation that leads to complex overall heat fluxes. Additionally, an air gap between rotor bell and mounting flange allows air- and heat-exchange, which makes the modeling even more challenging.

III. LUMPED PARAMETER THERMAL NETWORK

The selected lumped parameter thermal network to model the outer rotor SPM machine under test is depicted in Fig. 2. The illustrated cross section in Fig. 2a highlights the outer rotor bell structure that includes the rotor yoke and the permanent magnets, and the inner part of the machine that consists of the stator core and the windings, and the hollow stator fixture that connects the stator yoke to the mounting flange. The machine's shaft, which is connected to the rotor bell, is supported by ball bearings that are mounted in the inner part of the stator fixture. Preliminary analysis of the main heat flows allows reducing the cross section of the machine to simple geometric shapes and removing structures

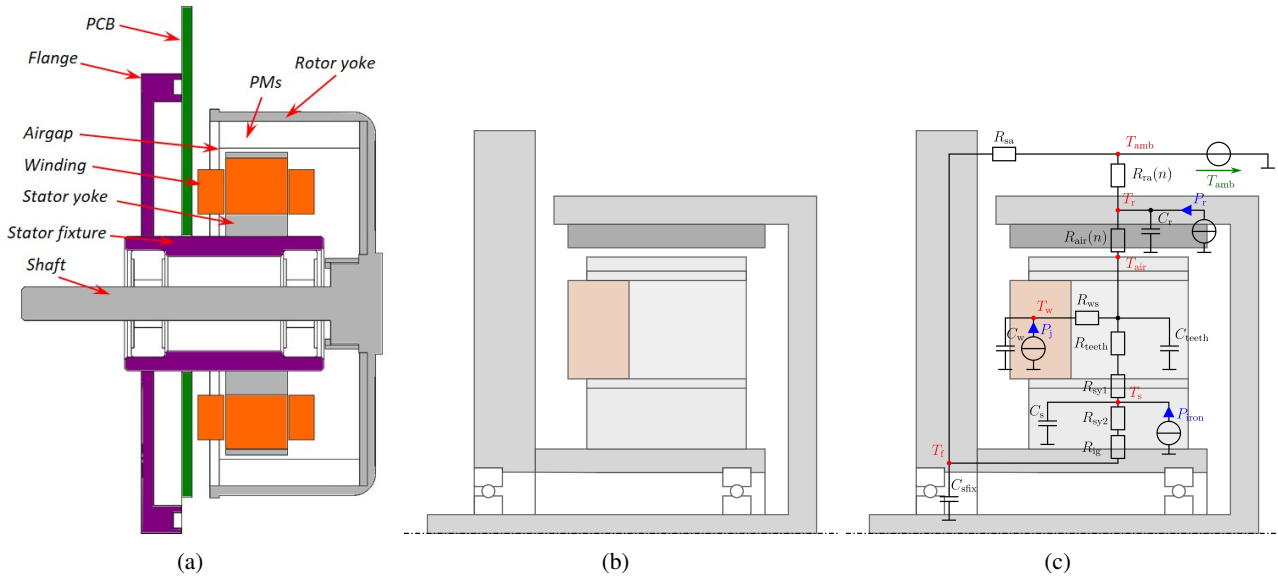


Fig. 2: Sketch of the circumferential cross section of the considered SPM outer rotor machine (a), the reduced motor cross section regarding thermal characteristics of the individual structures (b), and the correspondingly proposed lumped parameter thermal network - LPTN (c).

that can be neglected with respect to their thermal properties. This simplified geometry, shown in Fig. 2b, represents the basis of all further thermal modeling steps. Considering the axisymmetric geometry of the machine, Fig. 2c represents the five-node LPTN proposed for the thermal analysis of this outer rotor SPM machine. Considering a defined ambient temperature (T_{amb}), this thermal network allows evaluating the average temperatures of the rotor (T_r), the air gap (T_{air}), the stator winding (T_w), the stator yoke (T_s), and the stator fixture (T_f).

The current sources represent the heat sources related to the machine losses, i.e., the stator Joule (P_j) and iron (P_{iron}) losses, and the cumulative rotor losses (P_r). In order to limit the number of nodes and the complexity of the network, all the loss components in the machine can be reasonably linked to one of this three heat sources that are considered as uniformly distributed within their particularly associated component. For example, in the conducted analysis, P_r includes the magnets' and the rotor back iron losses. Accordingly, the heat source P_{iron} combines the iron losses in the stator lamination and friction losses in the bearings.

The thermal resistances constitute the different heat flow paths inside the machine and thus allow for computing the steady-state temperatures, while the thermal capacitances facilitate to further modeling the thermal transient behavior. If the machine's geometrical dimensions and the material properties are known, these network parameters can be reasonably approximated through using equations reported in literature [21]. In particular, the thermal capacitances of the stator teeth (C_{teeth}), stator yoke (C_s), stator fixture (C_{sf1x}) and of the rotor bell plus magnets (C_r) can be obtained by multiplying each the component's weight with the specific heat capacity of the applied materials, while the thermal resistances are usually computed considering the different machine parts as hollow

cylinders. It has to be emphasized that the entire machine arrangement features no symmetry the stator's axial center. Therefore, the adoption of the hollow cylinder theory for simplifying the thermal paths through teeth and stator yoke represents a rough approximation. In addition, the studied machine features a pancake shape where the end effects may result in non-negligible axial heat paths that affect the heat flows in radial direction. Nevertheless, the well-known hollow cylinder theory has been assumed as both a simple and practical approach for deriving start values for the thermal network parameters.

Looking at Fig. 2c, the thermal resistances R_{teeth} , R_{sy1} , and R_{sy2} define the thermal flux across the teeth and the stator yoke. In particular, the stator yoke has been subdivided into two parts, such that the stator iron losses are considered as impressed to the centre of the stator yoke. Through these elements, the heat transfer is mainly due to conduction, and the thermal resistances can thus be easily computed by using

$$R_{cond} = \frac{1}{2\pi k_{ir} L_s p_{ir}} \ln \left(\frac{r_{out}}{r_{in}} \right). \quad (1)$$

In (1), k_{ir} is the thermal conductivity coefficient of iron, L_s is the core length, and r_{in} and r_{out} are the inner and outer radii of the hollow cylinder that represents the considered machine part. The coefficient p_{ir} is the volume ratio between the stator teeth iron and the total teeth plus slot volume. For calculating the thermal resistance of a hollow cylinder without slots, e.g. R_{sy1} or R_{sy2} , the volume ratio p_{ir} is equal to one. In contrast, for an estimation of the thermal resistance of the teeth, R_{teeth} , values smaller 1 has to be used.

However, applying the knowledge of the geometrical or physical characteristics is not always straightforward as considered in Section III-A. For some LPTN parameters, e.g. the thermal resistance between winding and stator R_{ws} reliable

values can be obtained by means of accurate calibrations, based on DC tests or convection heat transfer and flow calculations [20], [21], [32].

A. Expert-based calibration of model parameters

The thermal resistance and capacitance of the stator winding cannot be easily computed because of the presence of air and non-uniformly distributed insulation layers between copper and iron, including resins and enamels. However, an equivalent thermal resistance (R_{ws}) and capacitance (C_w) between stator copper and stator iron can be obtained through a short-time DC thermal test according to the procedure described in [33]. Since the machine under test is delta-connected, the test has been executed supplying the current at two stator terminals. Hence, one phase is connected in parallel to the two remaining ones.

Additionally, the determination of the air gap thermal resistance is not trivial. The heat exchange between stator and rotor through the air gap can either be due to convection or radiation phenomena. Nevertheless, in previous activities related to induction motors, the authors verified that for thin air gap the thermal exchange can be equivalently modeled as a conductive thermal path in stationary air [21]. Since the machine under test features a small air gap thickness (0.5 mm) and the magnet is ring-shaped, also for this case the initial value for the air gap thermal resistance has been computed by using (1).

The heat exchange between the machine and external ambient is modeled through the thermal resistances R_{sa} and R_{ra} . Despite these parameters can be obtained by dedicated DC thermal tests as well, it is possible to approximate their values by analytical equations, as done by the authors for this research activity. R_{sa} embraces both the heat conduction along the stator fixture and the flange, as well as the convective heat exchange between the flange and the ambient. For the initial definition of the network parameters, the authors computed the conduction thermal resistance for the stator fixture indicated in Fig. 2a and properly increased this value based on author's experiences in order to consider the presence of the flange.

The thermal resistance R_{ra} that represents the heat exchange between the rotor bell and the ambient is rotor speed dependent. Considering standstill conditions, the heat flow is due to natural convection only, while during the rotation both natural and forced convection phenomena are present. The initial values for the network have been computed by the authors using well-known and proven empirical heat transfer correlations reported in literature [20], [32].

Regarding the interface gap thermal resistance R_{ig} , it could be estimated by either approximating the equivalent length of the interface gaps between stator yoke and stator fixture or, again, by means of a dedicated DC test. For the considered machine, the interface gap has been estimated to be approximately 30 μm , which corresponds to a typical value for interference fit assemblies according to authors experience.

All values of the computed or calibrated parameters in Section III-A of the assumed thermal network are summarized in Table III in Section V-D.

Torque-speed sensor	
Maximum rupture torque	1 N m
Maximum speed	50 000 rpm
Torque measurement range	± 200 mNm
Output voltage	± 5 V
Hysteresis brake	
Rated current (I_n)	270 mA
Min. torque at I_n	1.2 Nm
Maximum kinetic power	110 W
Maximum speed n_{\max}	12 000 rpm
Drag torque at n_{\max}	7.77 mNm

TABLE II: Main specifications for the torque-speed sensor and the hysteresis brake used for the experimental measurements.

IV. EXPERIMENTAL SETUP AND MEASUREMENT DATA

In order to verify the analytically derived thermal model, a test setup featuring an accurate measurement of the machine's temperatures is essential. In general, the transient temperature characteristics depend on the dynamic load profile that the machine is exposed to. Consequently, the experimental setup shown in Fig. 3a was designed for both the operation of the machine at different load points by controlling speed and torque, and a simultaneous acquisition of different temperatures within the machine. Its main components include the device under test (A), a hysteresis brake to apply various load points (B), a sensor to acquire speed and torque (C), and the power electronics including the inverter and a microcontroller (D) to apply a field-oriented control strategy of the machine under test to properly adjust the load point operation. Table II summarizes the key figures of the utilized torque-speed sensor and hysteresis brake.

A. Selected spots for the temperature monitoring

The transient temperatures of the individual motor components are determined via sensors at specific positions of interest. The internal structure of the motor, as well as the back side of the attached mounting flange are illustrated in Figs. 3b and 3c, respectively. For characterizing and monitoring the major thermal heat flow originated from different heat sources inside the device and towards the ambient, the following temperatures are acquired by thermal sensors:

- T_{uv} , T_{vw} , T_{wu} at the surface of one coil per phase;
- T_{air} at the tip of one pole shoe of the stator yoke;
- T_{bi} on the outer (static) ring of the inner ball bearing;
- T_{bo} on the outer (static) ring of the outer ball bearing;
- T_f on the mounting flange made of aluminum;
- T_r on the outer side of the rotor.

Their spatial positions inside the motor are illustrated in Figs. 3a-3c. All temperatures except T_r can be measured with conventional thermocouples of type K, which are connected to the relevant surface by using a thermally conductive adhesive. In contrast, the outer rotor temperature has to be measured by a contactless measuring method. For this purpose, a thermographic camera is used. Considering the given topology, the magnet's temperature cannot be directly measured.

B. Measurement results

In Fig. 4, sample data of one exemplary measurement cycle are presented. A stepwise random but reasonably bounded change of the load characterized by the respective torque and speed is considered. The transient characteristics of all eight acquired temperatures are recorded and are illustrated here. As can be observed, the winding temperatures are highest followed by the stator lamination. This is due to the fact that the Joule losses are the major loss component, especially if the load torque is high. Because of the surrounding air inside the bell following relatively low thermal heat exchange, the main heat flow applies from winding to the lamination. Nevertheless, especially for low load torques and high speeds, the amount of iron losses in the stator and the friction losses in the ball bearings cannot be neglected. For this reason, it would be an unreasonable oversimplification if the entire power loss is introduced through a single heat source, e.g. at the winding node P_j , for the whole speed and torque range. In general, the losses are generated at different positions in the motor. Consequently, a loss separation is discussed in the upcoming Section V-A, which facilitates subdividing the total losses into different heat sources in the network.

Generally, the thermocouple-based measurements show negligible measurement noise. This is different for the rotor temperature T_r , which is due to the measurement of said temperature along a rotating cylindrical device. Thus, any manufacturing tolerance affecting the rotor's true running accuracy, as well as a slightly different temperature distribution along the rotor housing's outer perimeter might cause this effect. Additionally, the thermographic camera has an auto-calibration feature that leads to a peak in the data approximately every three minutes.

V. PARAMETER OPTIMIZATION AND RESULTS

It was observed during modeling that the parameters R_{teeth} , R_{sy1} , R_{sy2} , and R_{ig} , that physically correspond to thermal conduction, can be determined with high accuracy based on expert knowledge. Furthermore, an individual weighting of

all machine components and the manufacturer's information about their material properties allow a precise estimation of the heat capacities C_r , C_{teeth} , C_s , and C_{sfix} . The parameters R_{ws} and C_w are calibrated by separate measurements described in Section III that particularly focus on the present winding configuration. By contrast, the quantities R_{air} , R_{sa} and R_{ra} are sensitive to the exact machine's manufacturing and their heat transport phenomena are usually a combination of natural and forced convection, as well as heat conduction. Thus, in the following they are selected as design parameters for a dedicated optimization problem. The parameter range is constrained based on expert knowledge to avoid potentially accurate solutions that are meaningless from a physical point of view.

A. Loss separation

As mentioned before, it is physically not correct to assign the entire amount of losses to the current source P_j in the network. For this reason, the measured total power losses P_{loss} presented in Fig. 4 have to be separated into Joule losses P_j associated with the ohmic resistance of the windings and residual losses P_{res} . The latter includes mechanical power loss induced by friction in the ball bearings and the iron losses in the laminated stator, the rotor iron, and the magnets, respectively. Assuming that the motor is symmetrical, $R_{uv} = R_{vw} = R_{wu}$ and $I_s = I_U = I_V = I_W$, the Joule losses can be estimated by

$$P_j = \frac{3}{2} I_s^2 R_{t,20} (1 + \alpha_{cu,20} (\bar{T}_w - 20^\circ\text{C})), \quad (2)$$

where I_s is the effective current measured by a power analyzer, $R_{t,20}$ is the terminal resistance at 20°C given in Table I, $\alpha_{cu,20}$ is the linear temperature coefficient of copper, and \bar{T}_w is the averaged winding temperature, as shown in Fig. 5. Consequently, the residual losses can be determined by $P_{\text{res}} = P_{\text{loss}} - P_j$. The subdivision of the residual losses P_{res} into the remaining power sources P_{iron} and P_r is very complex and generally depends on the current load point. To minimize the number of parameters to be optimized for the present analysis, a constant loss ratio $P_r = k_{p,\text{rot}} P_{\text{res}}$ and

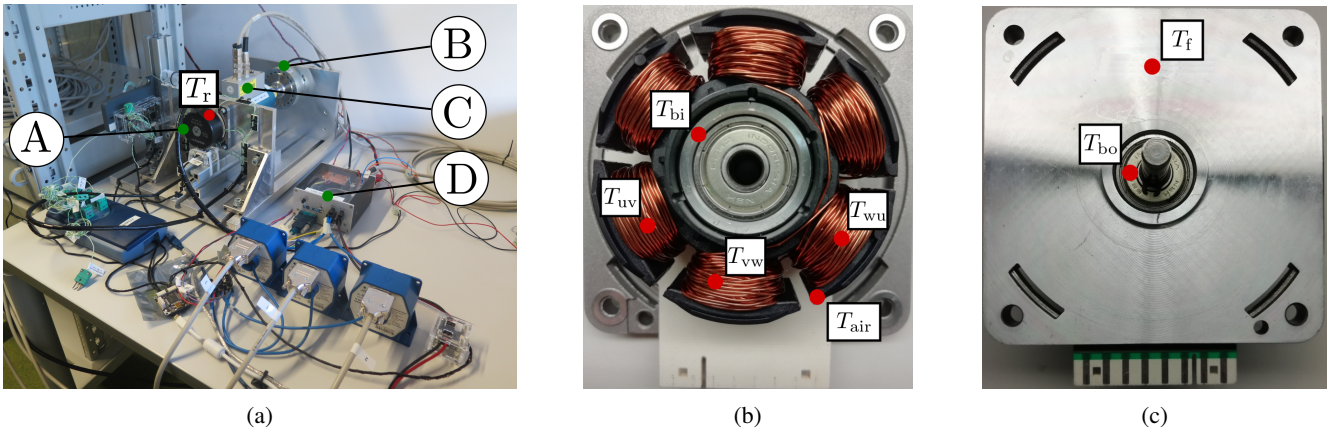


Fig. 3: (a) The test bench with the temperature measuring point T_r including the motor under test (A), the hysteresis brake (B), the speed-torque sensor (C) and the power electronics (D). (b) The stator front view and the considered temperature measuring points T_{uv} , T_{vw} , T_{wu} , T_{bi} , and T_{air} . (c) The flange back plate view with the positions of T_f and T_{bo} .

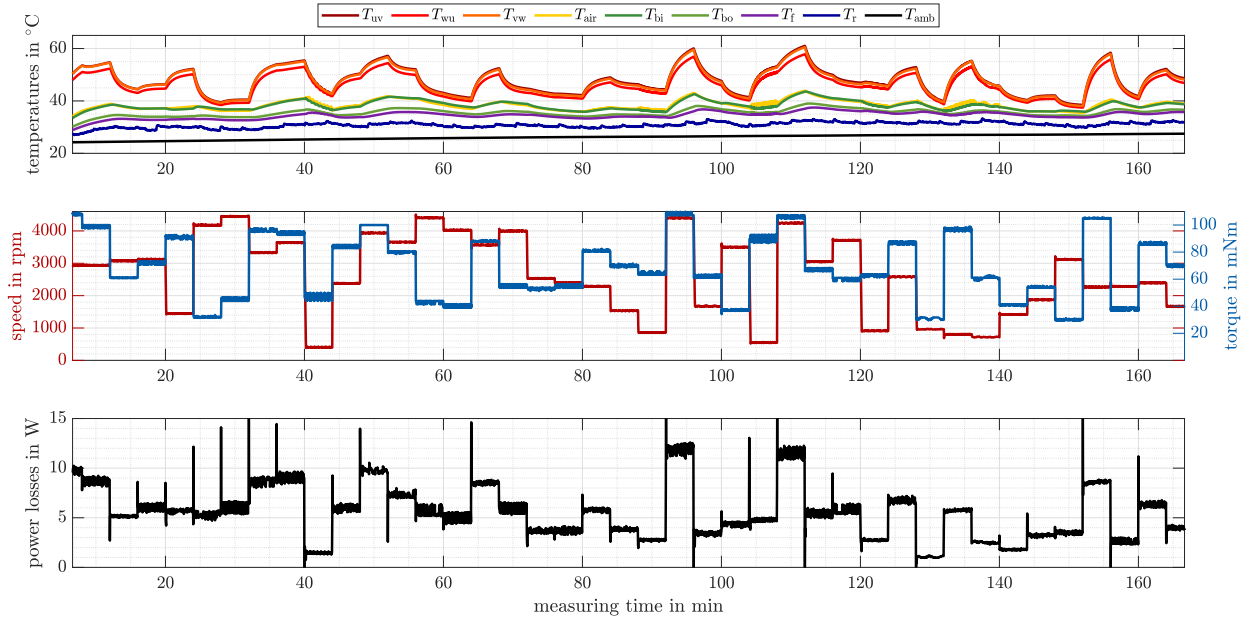


Fig. 4: A typical data set for transient load changes including the temperatures of all individual motor components, the speed and torque signals for applied transient load characteristics, and the total power loss of the motor.

$P_{\text{iron}} = (1 - k_{p,\text{rot}})P_{\text{res}}$, with the dimensionless parameter $k_{p,\text{rot}} = 0.1$ is chosen based on preliminary numerical simulations of the motor under test.

B. Speed dependent thermal resistances

All parameters analytically treated in Section III are derived on basic and simplified theories, e.g., by applying the hollow cylinder theory and general knowledge regarding convection on static cylinders and plates. However, measurements presented in Section IV show speed-dependent heating and cooling effects that cannot be covered by this simplified modeling approach. Hence, the speed-dependent behavior should be calibrated by using an optimization algorithm. In this analysis, a general linear speed dependency for a thermal resistance is considered by using

$$R_i(n) = R_{i,0} \left(1 - \frac{|n|}{n_{\max}} (1 - k_{i,s}) \right) + \Delta R_{i,0} \delta(n), \quad (3)$$

where n is the rotational speed of the rotor bell, $R_{i,0} = R_i(0)$ is the additive thermal resistance at zero speed, $n_{\max} =$

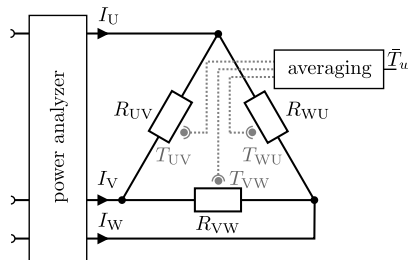


Fig. 5: Necessary measurements for loss separation including the currents, the electrical parameters of the machine and the recorded winding temperatures.

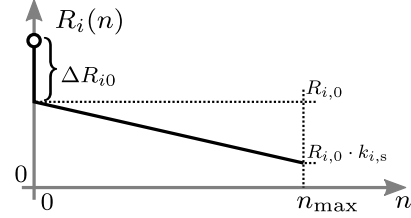


Fig. 6: Proposed function of a thermal resistance $R_i(n)$ depending on the speed of the rotor bell n .

7500 rpm is the maximum rotor speed, $k_{i,s}$ is the parameter to be optimized, and $\delta(n)$ is the delta-distribution. Within the subsequently presented optimization problem, the resistances representing the heat flow in the air gap, from rotor to ambient, and from stator to ambient are modeled as speed-dependent, thus $i = \{\text{air}, \text{ra}, \text{sa}\}$. The characteristics proposed in (3) are generally illustrated in Fig. 6. For this approach, only two parameters are required to be determined, which keeps the total parameter count reasonable. Nevertheless, both the high thermal resistance at standstill due to natural convection, as well as the decrease of thermal resistance because of forced convection at higher speeds can be represented with decent accuracy [20].

C. Applied optimizing technique

As a consequence, the uncertain parameters to be optimized are R_{sa} , R_{ig} , $R_{\text{ra},0}$, $R_{\text{air},0}$, $k_{\text{ra},s}$, $k_{\text{airgap},s}$, $\Delta R_{\text{ra},0}$, $\Delta R_{\text{air},0}$, and $\Delta R_{\text{sa},0}$. Thanks to the analytical approximations, a limitation of the design space is possible, but, nevertheless, the considered domain is high-dimensional. In order to find the global minimum and the corresponding best parameter setting, a genetic algorithm (GA) from the Java-based multi-objective optimization framework jmetal is applied [34]. This

type of algorithm is inspired by evolutionary principles from nature and can facilitate solving highly non-linear and multi-dimensional problems with regard to the number of design parameters and objectives [35]. Furthermore, the difficulty of selecting a collection of initial parameter sets is tackled by considering a Latin hypercube sampling (LHS) based approach. Hence, an initial set of parameter combinations fairly distributed within the design space is generated. In turn, it is utilized as start population for the genetic algorithm. A suitable cost function, i.e. the averaged RMS temperature error over all measured temperatures,

$$c = \sqrt{\frac{1}{M} \sum_{m=1}^M \frac{1}{N} \sum_{s=1}^N (T_{m,\text{mod}}[s] - T_{m,\text{meas}}[s])^2} \quad (4)$$

has been applied, where $T_{m,\text{mod}}[s]$ is the m -th temperature calculated by the model at time instant s , $T_{m,\text{meas}}[s]$ is the equivalent temperature measured using the experimental setup, N is the total number of samples, and M is the total number of considered temperatures within the optimization. This definition of the cost value can be interpreted as an averaged effective temperature error between calculated and measured temperatures. Consequently, a single-objective optimization problem was specified.

D. Optimization results and discussion

The LHS is used to randomly generate 4000 design variants before the GA is applied to minimize the cost functional (4), where at most 4000 more parameter settings are evaluated by utilizing a population size of 50 individuals. The presented optimization requires approximately 60 h on a desktop computer with 3.42 GHz clock frequency. Fig. 7 illustrates the evolution of the cost functional over evaluated samples for both the initial design of experiments and the subsequent optimization phase.

Figs. 8 and 9 show the measured temperature curves used for optimization compared with the modeling results. A combi-

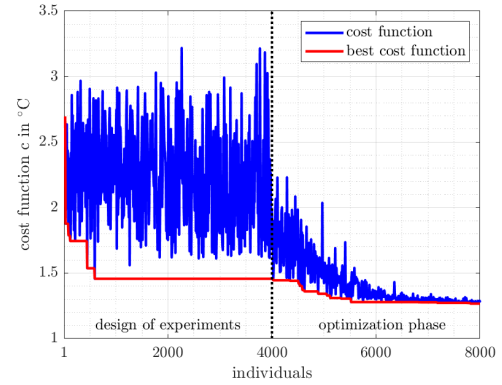


Fig. 7: Evolution of the cost function, i.e., the global effective temperature modeling error, with the number of evaluated parameter combinations.

nation of two different types of measurement runs, static ones with regard to eight different load points, and a dynamic load profile with 49 load steps, were considered. If the initial values are used without any adjustment, the cost function value, i.e. the average RMS temperature error, is $c_{\text{initial}} = 2.93^\circ\text{C}$.

According to Fig. 8, the initial network can model the dynamic variation of load points with high accuracy. As shown in the second diagram of Fig. 8, the residual of the temperatures varies in a range of -6°C and 8°C .

As presented in Fig. 9, the thermal network with optimized parameters models the static and the dynamic behavior of the motor more accurately. For this reason, the value of cost function is reduced to $c_{\text{opt}} = 1.28^\circ\text{C}$, which is about 2.3 times smaller compared to the initial setting. Additionally, the maximum error for both the static and the dynamic load variations is always within $\pm 4^\circ\text{C}$, and most of the time even smaller than $\pm 2.5^\circ\text{C}$.

Table III compares the initial values found by analytical approaches and the optimal parameters estimated through solving the particularly defined optimization problem. Looking

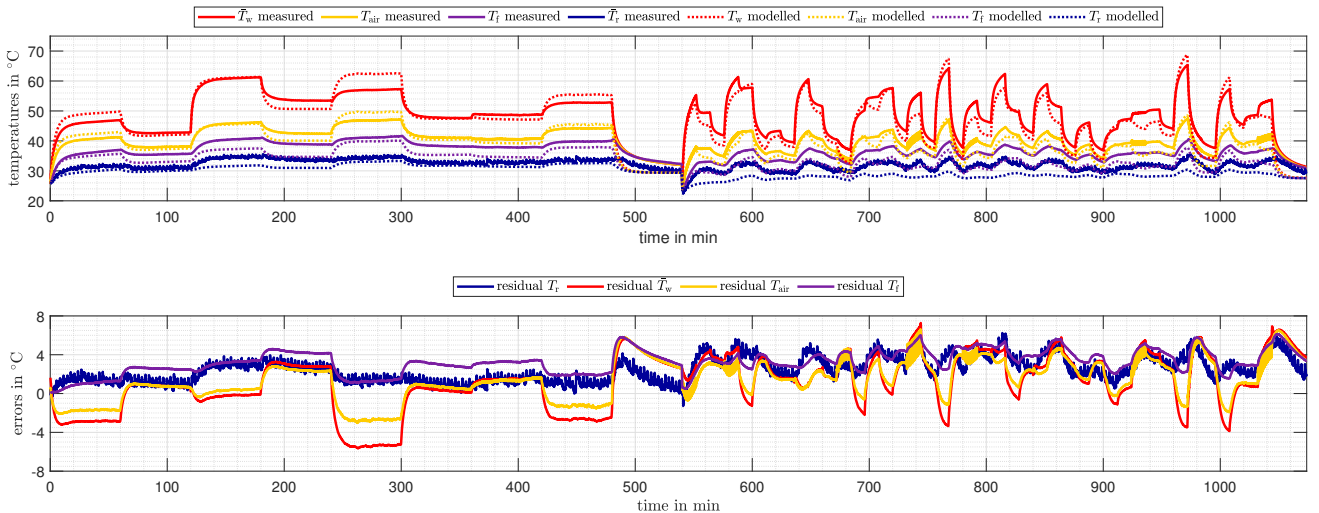


Fig. 8: Comparison of the measured temperature curves with those calculated by the thermal model **using the initial parameter set solely determined by analytical approaches** in Section III.

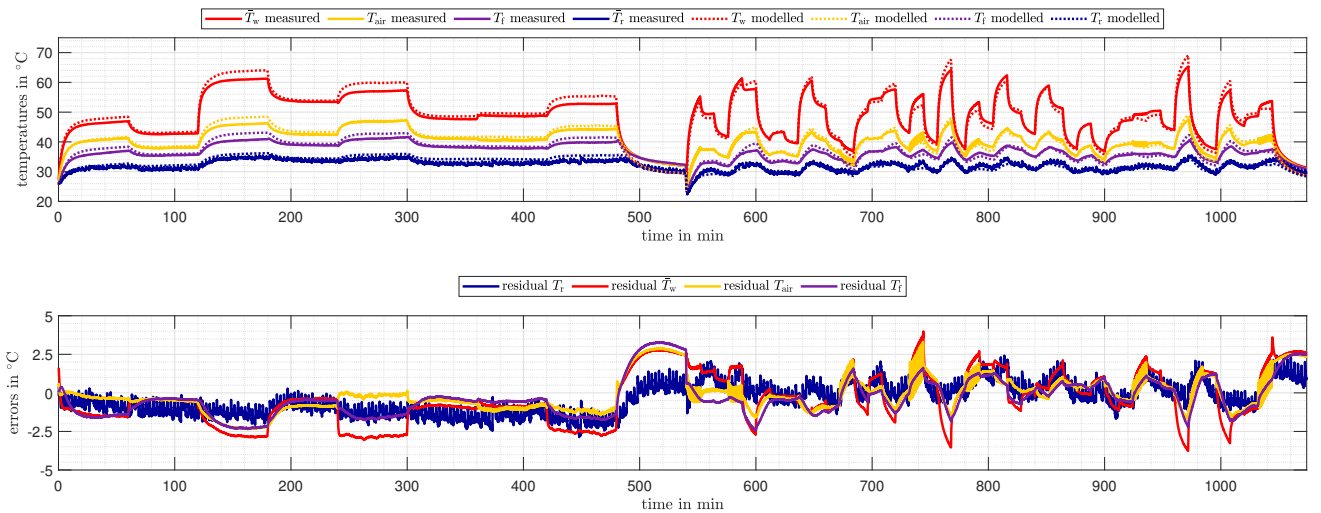


Fig. 9: Comparison of the measured temperature curves with those calculated by the thermal model **using the optimized parameter set** derived in Section V.

at the table it is possible to appreciate that the initial values computed as described in Section III are a reliable starting point for solving the optimization problem. However, the bigger differences between initial and optimized values have been noted for the convective thermal resistances $R_{air,0}$ and R_{sa} parameters that are prone to large deviation by the assumptions of the hollow cylinder theory, in particular for machines characterized by a small axial length / diameter ratio.

Additionally, a general modeling theorem is that it is essential to validate any modeling approach by additional data not available at the modeling stage, i.e., so called data for validation. Accordingly, further measurement cycles were run, featuring random dynamic load profiles. In addition, a very long cooling phase was introduced at the end of the load cycle, as previous experience showed that such periods often are hard to predict, especially if they are not present within the modeling data. In Fig. 10, the achieved results are presented. As can be seen, the model's fidelity is excellent, revealing a

very low absolute error in temperature prediction, which is smaller than 2.5°C for any of the investigated temperature spots. This further holds for nearly all time instants within the 134 hours of recorded data sets.

Regarding Fig. 9, the modeling error is larger at higher temperatures, e.g., cf. winding temperature for the time between minute 240 and 300. On the one hand, this could either be related to the limited data available in this temperature range. Consequently, such load points would be underrepresented in the optimization scenario, leaving the error in this range unconsidered. On the other hand, it could be a fundamental error due to the assumptions made for modeling thermal resistances or a wrong network topology.

Thus, a more detailed analysis was performed, that is reported in the following: Therefore, the trajectory of load points was recorded, which are specified by their speed and torque. It is illustrated in Fig. 11. Besides some boundaries regarding minimum values for speed and torque given by

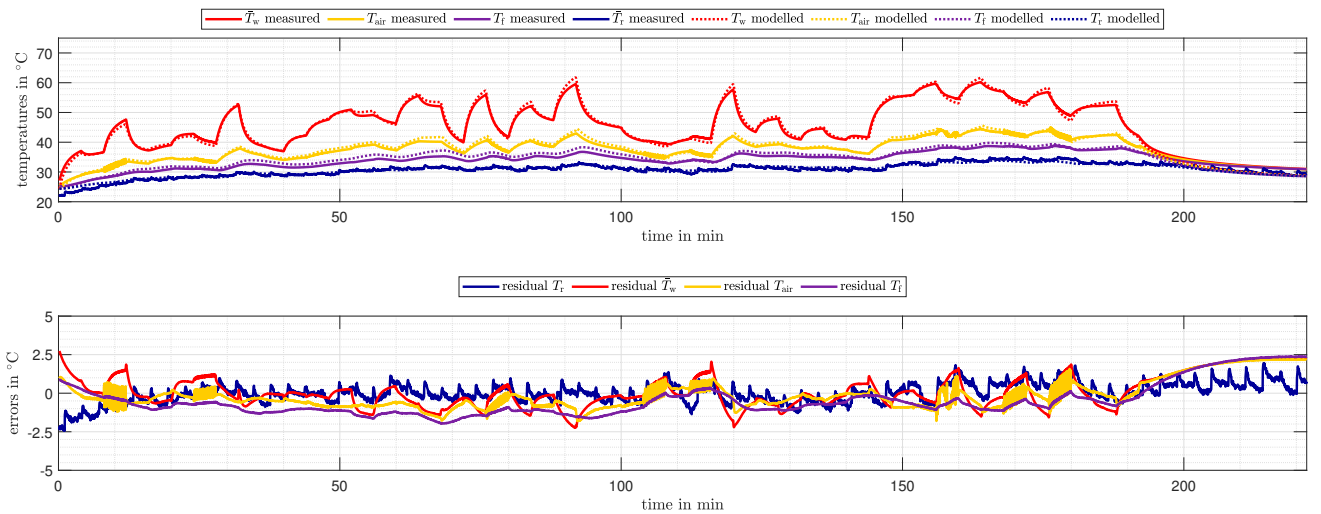


Fig. 10: **Evaluation** of the thermal model with **measured temperature curves not used for the parameter optimization**.

Parameter at 20 °C	Initial value	Optimized value
R_{heeth}	0.24 K W^{-1}	
R_{sy1}	0.024 K W^{-1}	
R_{sy2}	0.028 K W^{-1}	
R_{ig}	1.00 K W^{-1}	1.34 K W^{-1}
R_{ws}	2.75 K W^{-1}	
$R_{\text{air},0}$	11.3 K W^{-1}	4.11 K W^{-1}
$R_{\text{ra},0}$	1.74 K W^{-1}	2.28 K W^{-1}
R_{sa}	1.20 K W^{-1}	3.79 K W^{-1}
C_r	122 J K^{-1}	
C_{teeth}	31.4 J K^{-1}	
C_s	27.7 J K^{-1}	
C_{sfix}	125 J K^{-1}	
C_w	19.8 J K^{-1}	
$k_{\text{ra,s}}$	1.0	0.13
$k_{\text{airgap,s}}$	1.0	0.18
$\Delta R_{\text{ra},0}$	0.0 K W^{-1}	3.43 K W^{-1}
$\Delta R_{\text{air},0}$	0.0 K W^{-1}	1.25 K W^{-1}
$\Delta R_{\text{sa},0}$	0.0 K W^{-1}	14.1 K W^{-1}

TABLE III: Comparison of the analytically determined and the optimized parameter set

dashed lines, the permissible area for the motor operation is further constrained by the black solid lines, characterizing a speed-dependent maximally possible load torque. Thanks to an increase in the cooling effect, the permitted torque even increases with speed up to nearly 6000 rpm, while subsequently it must be reduced for even higher rotational velocities. As can be seen, particularly the high speed region and, to some extent, the higher torque region is underrepresented within the available data.

In order to evaluate the regions of most significant modeling errors, a corresponding heat map was derived. It is presented in Fig. 12. While the two axes, again, represent the speed and torque, the color within certain speed-/torque-regions illustrates the associated modeling error, which ranges from blue (0K) up to dark red (4K). A Gaussian blurring filter was used to reduce measurement noise and smooth transitions between neighboring regions. From this visualization, it becomes evident that especially the underrepresented areas

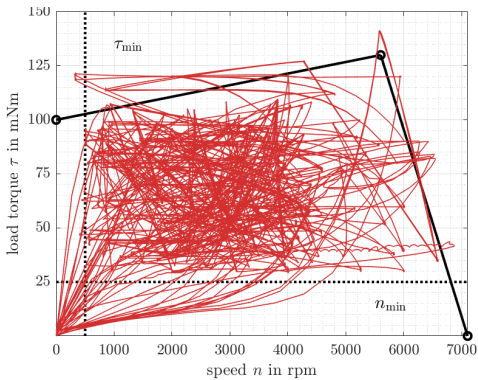


Fig. 11: Trajectory for sampling the speed-/torque-domain - all recorded measurement cycles are plotted.

regarding the trajectory in Fig. 11 show the most significant modeling errors. This can mainly be due to two reasons, (i): the modeling generally does not allow more accurate results for this region, or (ii): due to the under-representation of the respective speed-/torque-domains, the other regions are more pronounced and thus a small modeling error for that regions is more beneficial for reducing the cost function. Most likely, (ii) applies here. Future analyses shall be about investigating and comparing different cost functionals, and focusing on the data selection to evenly represent all relevant domains. Besides, investigating multi-objective problems regarding the different machine components' temperatures and their respective errors can provide further insight to limitations and potential improvements for the structure of the proposed network and the speed- and temperature dependency of the heat transfer [36].

Generally, it can be concluded that the proposed modeling approach is highly suited for observing the thermal state of the machine components during operation without any temperature sensors needed. Besides, a very high modeling fidelity was achieved, while the model's complexity is still low. Thus, it could be implemented either for real time temperature evaluation using a desktop computer, or by running it on a digital signal processor (DSP). Potential applications can be temperature monitoring in general, predictive maintenance, or an active derating based on the load history the electric machine was exposed to. Running the model on the DSP is the future goal of the authors in order to further highlight the applicability and usefulness of the proposed modeling.

VI. CONCLUSION

This paper gives an overview about measurement-based optimization of a thermal model for an outer rotor PM machine. First, an initial physics-based lumped parameter thermal network featuring resistances and capacitances is introduced. The initial parameters of the network are determined based on analytical approaches, or, in the case of convective heat transfer, roughly estimated. Consequently, the more uncertain parameters are optimized by using a genetic algorithm with a Latin hypercube sampling-based start-up phase based on experimentally acquired data. Additionally, a loss separation and a speed-dependent modeling of convective heat transitions are introduced. Through the optimization process, the

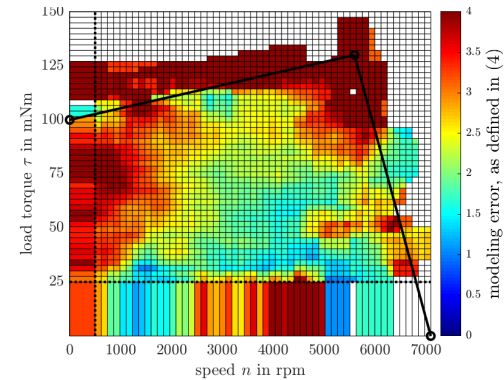


Fig. 12: Heat map of the speed-/torque-dependent modeling error, according to the definition provided in (4).

mean effective temperature error is reduced by a factor of 2.3. This practically follows maximum temperature errors of about 2.5K for almost any time instant within the 134 hours of recorded data. In future works, the aim is to further improve the modeling accuracy by considering a speed- and temperature-dependent loss separation, as well as to implement the derived model on a digital signal processor to apply it for condition monitoring, predictive maintenance, or active de- or uprating. Additionally, the generality of the proposed approach regarding the thermal modeling of larger outer-rotor machines for higher output power will be investigated, taking into account that these machines generally adopt different materials, manufacturing techniques and cooling solutions with respect to sub-kW machines.

REFERENCES

- [1] D. Wöckinger, G. Bramerdorfer, S. Drexler, S. Vaschetto, A. Cavagnino, A. Tenconi, W. Amrhein, and F. Jeske, "Measurement-based optimization of thermal networks for temperature monitoring of outer rotor pm machines," in *2020 IEEE Energy Conversion Congress and Exposition (ECCE)*, Oct 2020, pp. 4261–4268.
- [2] B. Fahimi, O. Mohammed, H. Toliaty, J. Kirtley, S. Pekarek, L. Parsa, K. Hameyer, A. Sarikhani, E. Muljadi, and J. Hendershot, "Guest Editorial Optimal Design of Electric Machines," *IEEE Transactions on Energy Conversion*, vol. 30, no. 3, pp. 1143–1143, sep 2015.
- [3] G. Bramerdorfer, J. A. Tapia, J. J. Pyrhönen, and A. Cavagnino, "Modern Electrical Machine Design Optimization: Techniques, Trends, and Best Practices," *IEEE Transactions on Industrial Electronics*, vol. 65, no. 10, pp. 7672–7684, 2018.
- [4] A. Cavagnino, G. Bramerdorfer, and J. A. Tapia, "Optimization of electric machine Designs - Part I," *IEEE Transactions on Industrial Electronics*, vol. 64, no. 12, pp. 9716 – 9720, 2017.
- [5] A. Cavagnino, G. Bramerdorfer, and J. A. Tapia, "Optimization of Electric Machine Designs - Part II," *IEEE Transactions on Industrial Electronics*, vol. 65, no. 2, pp. 1700–1703, 2017.
- [6] A. Fatemi, D. M. Ionel, M. Popescu, Y. C. Chong, and N. A. O. Demerdash, "Design Optimization of a High Torque Density Spoke-Type PM Motor for a Formula E Race Drive Cycle," *IEEE Transactions on Industry Applications*, vol. 54, no. 5, pp. 4343–4354, sep 2018.
- [7] M. Popescu, I. Foley, D. A. Staton, and J. E. Goss, "Multi-physics analysis of a high torque density motor for electric racing cars," *2015 IEEE En. Conv. Congr. and Exp. (ECCE)*, pp. 6537–6544, Sep. 2015.
- [8] L. Sobotka, R. Pechanek, and L. Veg, "Coupled Transient Thermal Analyses of Passive Cooling Traction PMSM from the Racing Formula," in *2021 IEEE 19th International Power Electronics and Motion Control Conference (PEMC)*. IEEE, apr 2021, pp. 426–432.
- [9] G. Lei, T. Wang, J. Zhu, Y. Guo, and S. Wang, "System-Level Design Optimization Method for Electrical Drive Systems—Robust Approach," *IEEE Transactions on Ind. El.*, vol. 62, no. 8, pp. 4702–4713, aug 2015.
- [10] F. Zhang, D. Gerada, Z. Xu, C. Liu, H. Zhang, T. Zou, Y. C. Chong, and C. Gerada, "A Thermal Modeling Approach and Experimental Validation for an Oil Spray-Cooled Hairpin Winding Mach." *IEEE Trans. on Transp. Electr.*, vol. 7, no. 4, pp. 2914–2926, dec 2021.
- [11] F. Hoffmann, D. Silys, and M. Doppelbauer, "Transient Thermal Model for Ball Bearings in Electrical Machines," in *2020 Intern. Conf. on Electr. Mach. (ICEM)*. IEEE, aug 2020, pp. 1018–1024.
- [12] Y. Shi, J. Wang, R. Hu, and B. Wang, "Electromagnetic and Thermal Behavior of a Triple Redundant 9-Phase PMASynRM With Insulation Deterioration Fault," *IEEE Transactions on Industry Applications*, vol. 56, no. 6, pp. 6374–6383, nov 2020.
- [13] F. Hoffmann, S. Foitzik, and M. Doppelbauer, "Thermal 3D Modeling and Analysis of PMSMs with Inter-Turn Faults," in *2021 IEEE Intern. Electr. Mach. & Dr. Conf. (IEMDC)*. IEEE, may 2021, pp. 1–7.
- [14] X. Yi, T. Yang, J. Xiao, N. Miljkovic, W. P. King, and K. S. Haran, "Equivalent Thermal Conductivity Prediction of Form-Wound Windings With Litz Wire Including Transposition Effects," *IEEE Transactions on Industry Applications*, vol. 57, no. 2, pp. 1440–1449, mar 2021.
- [15] V. V. Ryzhov, O. N. Molokanov, P. A. Dergachev, S. V. Osipkin, E. P. Kurbatova, and P. A. Kurbatov, "Three-dimensional Mathematical Simulation of the Stator Slot of a Turbogenerator, Including Thermal Modeling and Flow Fluid Dynamics," in *2021 17th Conf. on El. Mach., Drives and Power Syst. (ELMA)*, no. July. IEEE, jul 2021, pp. 1–4.
- [16] R. Pechanek, M. Skalicky, and J. Drazen, "Determinations of Stator Windings Thermal Model with Various Filling Factor," in *2020 19th Intern. Conf. on Mechan. - Mechatronika*, dec 2020, pp. 1–6.
- [17] B. Assaad, K. El Kadri Benkara, G. Friedrich, S. Vivier, and A. Michon, "Reducing the complexity of thermal models for electric machines via sensitivity analyses," *2017 IEEE Energy Conversion Congress and Exposition, ECCE 2017*, vol. 2017-Janua, pp. 4658–4665, 2017.
- [18] Z. Sheng, H. Lin, and D. Wang, "A kind of node number selection method for electrical machine lumped-parameter thermal model based on the systematic bias," in *20th IEEE Intersoc. Conf. on Therm. and Thermom.. Phen. in Electr. Syst. (iTherm)*, jun 2021, pp. 154–161.
- [19] W. Zhao, D. Cao, J. Ji, L. Huang, and T. Liu, "A Generalized Mesh-Based Thermal Network Model for SPM Machines Combining Coupled Winding Solution," *IEEE Trans. on Ind. El.*, vol. 68, no. 1, pp. 116–127, jan 2021.
- [20] D. A. Staton and A. Cavagnino, "Convection heat transfer and flow calculations suitable for electric machines thermal models," *IEEE Transactions on Industrial Electronics*, 2008.
- [21] A. Boglietti, A. Cavagnino, M. Lazzari, and M. Pastorelli, "A Simplified Thermal Model for Variable-Speed Self-Cooled Industrial Induction Motor," *IEEE Transactions on Industry Applications*, 2003.
- [22] P. Giangrande, V. Madonna, S. Nuzzo, C. Spagnolo, C. Gerada, and M. Galea, "Reduced order lumped parameter thermal network for dual three-phase permanent magnet machines," *2019 IEEE Worksh. on El. Mach. Design, Contr. and Diagn. (WEMDCD)*, vol. 1, pp. 71–76, 2019.
- [23] M. Popescu, D. A. Staton, A. Boglietti, A. Cavagnino, D. Hawkins, and J. Goss, "Modern Heat Extraction Systems for Power Traction Machines - A Review," *IEEE Transactions on Industry Applications*, 2016.
- [24] F. Boseniu and B. Ponick, "Parameterization of transient thermal models for permanent magnet synchronous machines exclusively based on measurements," *2014 Intern. Symp. on Power Electr., Electr. Drives, Automation and Motion, SPEEDAM 2014*, pp. 295–301, 2014.
- [25] L. Ma, L. Zhao, and X. Wang, "Prediction of thermal system parameters based on PSO-ELM hybrid algorithm," *Proc. - 2017 Chinese Automation Congr., CAC 2017*, pp. 3136–3141, 2017.
- [26] W. Kirchgassner, O. Wallscheid, and J. Böcker, "Deep residual convolutional and recurrent neural networks for temperature estimation in permanent magnet synchronous motors," *2019 IEEE Intern. Electr. Mach. and Drives Conf., IEMDC*, pp. 1439–1446, 2019.
- [27] Z. Xu, Y. Gao, X. Wang, X. Tao, and Q. Xu, "Surrogate Thermal Model for Power Electronic Modules using Artificial Neural Network," in *IECON 2019 - 45th Annual Conference of the IEEE Industrial Electronics Society*, vol. 1. IEEE, oct 2019, pp. 3160–3165.
- [28] K. Zhang, A. Giuliani, S. Ogreni-Memik, G. Memik, K. Yoshii, R. Sankaran, and P. Beckman, "Machine Learning-Based Temperature Prediction for Runtime Thermal Management Across System Components," *IEEE Trans. on Par. and Distr. Syst.*, vol. 29, no. 2, pp. 405–419, 2018.
- [29] E. Breitenbach, E. Wunsch, and A. Schramm, "Thermal Monitoring of Electrical Machines by Linear Differential Equations and Numerical Calibration Procedure," in *2020 Intern. Symp. on Power El., El. Drives, Autom. and Motion (SPEEDAM)*, jun 2020, pp. 168–172.
- [30] G. Guedia Guemo, P. Chantrenne, and J. Jac, "Parameter identification of a lumped parameter thermal model for a permanent magnet synchronous machine," *Proceedings of the 2013 IEEE International Electric Machines and Drives Conference, IEMDC 2013*, pp. 1316–1320, 2013.
- [31] C. Sciascera, P. Giangrande, L. Papini, C. Gerada, and M. Galea, "Analytical Thermal Model for Fast Stator Winding Temperature Prediction," *IEEE Trans. on Ind. El.*, vol. 64, no. 8, pp. 6116–6126, aug 2017.
- [32] D. Staton, A. Boglietti, and A. Cavagnino, "Solving the More Difficult Aspects of Electric Motor Thermal Analysis in Small and Medium Size Industrial Induction Motors," *IEEE Transactions on Energy Conversion*, vol. 20, no. 3, pp. 620–628, sep 2005.
- [33] A. Boglietti, M. Cossale, S. Vaschetto, and T. Dutra, "Thermal Conductivity Evaluation of Fractional-Slot Concentrated-Winding Machines," *IEEE Trans. on Ind. Appl.*, vol. 53, no. 3, pp. 2059–2065, 2017.
- [34] J. J. Durillo and A. J. Nebro, "jmetal: A java framework for multi-objective optimization," *Adv. in Eng. Softw.*, vol. 42, pp. 760–771, 2011.
- [35] M. Mitchell, *An Introduction to Genetic Algorithms*. Cambridge, MA, USA: MIT Press, 1996.
- [36] D. Wöckinger, G. Bramerdorfer, S. Vaschetto, A. Cavagnino, A. Tenconi, W. Amrhein, and F. Jeskey, "Approaches for improving lumped parameter thermal networks for outer rotor spm machines," in *2021 IEEE Energy Conversion Congress and Exposition (ECCE)*, Oct 2021, pp. 9821–9826. <https://creativecommons.org/licenses/by/4.0/>